DEUTSCHES ELEKTRONEN-SYNCHROTRON DESY

DESY SR-77/12
July 1977

X-Ray Energy-Dispersive Diffractometry Using Synchrotron Radiation

by

B. Buras and J. Staun Olsen

Physics Laboratory II, University of Copenhagen, Universitetsparken 5, DK-2100 Copenhagen, Denmark

L. Gerward

Laboratory of Applied Physics III, Building 307, Technical University of Denmark, DK-2800 Lyngby, Denmark

G. Will and E. Hinze

Mineralogical Institute, University of Bonn, Bonn, Federal Republic of Germany

NOTKESTRASSE 85 · 2 HAMBURG 52

To be sure that your preprints are promptly included in the
HIGH ENERGY PHYSICS INDEX ,
send them to the following address (if possible by air mail) :

DESY
Bibliothek
Notkestraße 85
2 Hamburg 52
Germany

X-Ray Energy-Dispersive Diffractometry Using Synchrotron Radiation

BY B. BURAS*) AND J. STAUN OLSEN

Physics Laboratory II, University of Copenhagen,
Universitetsparken 5, DK-2100 Copenhagen, Denmark.

L. GERWARD

Laboratory of Applied Physics III, Building 307,
Technical University of Denmark, DK-2800 Lyngby, Denmark,

AND G. WILL AND E. HINZE

Mineralogical Institute, University of Bonn,
Bonn, Federal Republic of Germany.

Accepted for publication in Journal of Applied Crystallography.

Abstract

The special features of X-ray energy-dispersive powder and single crystal diffraction using synchrotron radiation are discussed on the basis of experiments performed at the Deutsches Elektronen-Synchrotron, DESY. The method is shown to be of particular value for fast structure identifications, experiments for which large scattering vectors are important, studies of phase transformations and chemical reactions at elevated temperatures and high-pressure studies. Studies of time-dependent phenomena using pulsed external fields are discussed.

*)Also at Research Establishment Risø, DK-4000 Roskilde, Denmark.

1. Introduction

The energy-dispersive method has developed into a useful tool for powder and single crystal diffraction (Giessen & Gordon, 1968; Buras, Chwaszczewska, Szarras & Szmid, 1968; Läine, Lähteenmäki & Pääkkäinen, 1974; Buras, Staun Olsen, Gerward, Selsmark & Lindegaard-Andersen, 1975; and references therein). In this method a continuous incident X-ray spectrum and a fixed scattering angle, $2\theta_0$, are used. The relation between the interplanar spacing, d_H, and the energy, E_H, of the scattered photons is given by (Cole, 1970)

$$E_H \, d_H \sin\theta_0 = hc = 6.199 \ (\text{keV}\cdot\text{Å}) \ , \qquad (1)$$

where H denotes hkl.

Until very recently, Bremsstrahlung from an X-ray tube has been used exclusively as the source of white radiation for the energy-dispersive method. However, this radiation has some disadvantages: (a) the intensity is modest, (b) the continuous spectrum is accompanied by monochromatic (in this case) characteristic radiation, (c) the polarization is energy dependent in a manner difficult both to measure and to calculate (Buras, Gerward, Selsmark, Buras & Staun Olsen, 1975), and (d) the range of useful energies (wavelengths) is limited.

In contrast to Bremsstrahlung from X-ray tubes, synchrotron radiation is very intense, has a smooth spectrum, and a well defined polarization. The range of useful energies can be extended to 70 keV and higher depending on the properties of the synchrotron. In addition, the X-ray beam is very well collimated. Thus synchrotron radiation seems to be an ideal X-ray source for energy-dispersive diffractometry. This was recently demonstrated both for powder diffraction (Buras, Staun Olsen & Gerward, 1976) and for small-angle scattering (Bordas, Munro & Glazer, 1976).

The present paper describes methodological studies performed at the Deutsches Elektronen-Synchrotron, DESY, with the aim to find out the special features of the energy-dispersive method using synchrotron radiation as the X-ray source. The experimental arrangement is described in §2. Resolution and integrated intensities are discussed in §3 and 4, followed by an analysis of short-time exposures (§5). The use of large scattering vectors is discussed in §6. Results of experiments on samples subjected to different controlled environments are shown in §7 through 9. In §7 a phase transformation and a chemical reaction at elevated temperatures are followed. High-pressure experiments are described in §8. The interesting possibility of studying time-dependent phenomena using pulsed external fields in combination with the pulsed synchrotron radiation is discussed in §9. Finally, a brief summary is given in §10.

2. Experimental

A portable, remote-controlled diffractometer was constructed and transported to DESY for the experiments (Fig. 1). Powdered samples as well as single crystals could be placed and adjusted on the goniometer. Facilities were provided for mounting an oven (50-850 °C ± 0.25 °C in He atmosphere) and a high-pressure cell. Details of the experimental arrangement and a comparison between diffraction spectra recorded by a Si(Li) detector and a pure Ge detector have been published elsewhere (Buras, Staun Olsen & Gerward, 1976). The experiments were made when the synchrotron was run with a maximum electron energy of 6.66 and 7.22 GeV. The electron current was between 7 and 10 mA.

Special care was taken to avoid saturation effects in the detector system. This is especially important as DESY is a pulsed X-ray source with a repetition rate of 50 Hz and an X-ray pulse width of ca. 3 ms*). Thus a collection of about 6000 counts in 1 s corresponds to about 40000 c/s in

---

*) We are not discussing the fine structure of this pulse.

the pulse. This counting rate could be measured with our equipment with a deadtime of 10%. A more sophisticated electronic detector system is required for more efficient use of the high intensity of the synchrotron radiation.

3. Resolution

The resolution, D_H, is here defined as

$$D_H = (\Delta E/E)_H \ , \qquad (2)$$

where ΔE is the full width at half maximum of the hkℓ reflection in the energy scale. There are two terms contributing to D_H: the energy resolution, δE, of the semiconductor detector and amplifier, and the geometrical term, $\cot \theta_0 \ \Delta\theta_0$, due to the finite collimation of the incident and scattered beams. Thus

$$D_H = \left[(\delta E/E)_H^2 + (\cot \theta_0 \ \Delta\theta_0)^2\right]^{\frac{1}{2}} \ . \qquad (3)$$

Note that the first term is energy dependent (also because δE is a slowly increasing function of E) and the second term energy independent.

Figure 2 shows the measured resolution as a function of photon energy for two powder patterns. The experimental points lie on the same curve although the scattering angles differ. This indicates that the geometrical

term is small. In fact, the incident beam has a divergence of 0.1 mrad and the divergence of the scattered beam is 0.9 mrad and so $\Delta\theta_0 \approx 1$ mrad. This gives the values 0.0033 and 0.0025, respectively, for the geometrical term. Both these values are in our case smaller than $\delta E/E$ in the whole energy range used here. Thus, in view of equation (3), the contribution of the geometrical term to the total resolution is negligible. Other examples analyzed by us show the same feature (except for small-angle scattering).

Hence the limiting factor is the energy resolution of the detector system. As seen in Fig. 2, the resolution is 1.5-2% in the range 10-20 keV, but for energies larger than about 30 keV it is below 1%. In this connection it should be noticed that the resolution is better for the large index reflections, where it is usually far more necessary than for the small index reflections.

4. Integrated intensities and structure factors; intensity and polarization of the synchrotron radiation

4.1. Integrated intensities of Bragg reflections.

Theoretical expressions for the integrated intensities to be used in the energy-dispersive method have been given by Buras and Gerward (1975). For powered crystals, it follows from those expressions that the integrated

intensity, I_H, recorded by the detector is given by

$$I_H = Cn(E)i_0(E)j_H d_H^2 |F_H|^2 A(E,\theta_0) C_p / \sin\theta_0 \ , \qquad (4)$$

where C is a constant, $n(E)$ the detector efficiency, $i_0(E)$ the intensity per unit energy range of the incident beam, j_H the multiplicity factor, F_H the structure factor, $A(E,\theta_0)$ the absorption factor, and C_p the polarization factor. For a single crystal, one has in the kinematical approximation (negligible primary and secondary extinction):

$$I_H = C'n(E)i_0(E)d_H^2 |F_H|^2 A(E,\theta_0) C_p \ , \qquad (5)$$

where C' is a constant.

The polarization factor that appears in equations (4) and (5) is given by

$$C_p = (i_{0,n}(E) + i_{0,p}(E)\cos^2 2\theta_0)/i_0(E) \ , \qquad (6)$$

where $i_{0,n}$ and $i_{0,p}$ are the intensities of the normal and parallel components of the incident beam with respect to the scattering plane*), and $i_{0,n} + i_{0,p} = i_0$. Thus C_p is a function of E and θ_0.

*) The scattering plane is defined by the incident and scattered beam directions.

For a large perfect crystal, the dynamical theory of diffraction should be used. In the present work we will make the simplifying assumptions of a symmetric Bragg reflection and a negligibly small true absorption (the Darwin solution). In this case the H- and θ_0-dependent factors can be separated and one obtains (Buras et al., 1975):

$$I_H = C''n(E)i_0(E)d_H |F_H| C_p(\mathrm{dyn}) / \sin\theta_0 \ , \qquad (7)$$

where C'' is a constant. The polarization factor is now given by

$$C_p(\mathrm{dyn}) = (i_{0,n}(E) + i_{0,p}(E)|\cos 2\theta_0|)/i_0(E) \ . \qquad (8)$$

4.2. Intensity and polarization of the synchrotron radiation.

The intensity and polarization of the radiation emitted by the accelerated electrons in the synchrotron can be calculated using relativistic electromagnetic theory. Figure 3 shows the spectral distribution, $i_0(E)$, of synchrotron radiation for the maximum electron energy 6.66 GeV, beam current 7 mA and a rectangular slit, 4 mm high and 0.8 mm wide, at a distance of 40 m from the focus point. Curve a shows the intensity in vacuum obtained with a computer program developed at DESY (Koch & Kunz, 1974). The beryllium window, 0.25 mm thick, at the end of the beam pipe cuts off the intensity for energies below 3.5 keV, as shown by curve b. Finally, curve c shows

the attenuation due to a 1 m beam path in air after the beryllium window. The difference between curves b and c indicates that whenever long beam paths are necessary, it might be advisable to use evacuated or helium-filled beam pipes.

The synchrotron radiation is linearly polarized to 100 % in the orbit plane with the electric field vector parallel to this plane. Above and below the orbit plane a vertical component appears, but it is very small in the X-ray range. The polarization, P, is defined in the usual way:

$$P(E) = (i_{0,||}(E) - i_{0,\perp}(E)) / i_0(E) \quad , \tag{9}$$

where $i_{0,||}$ and $i_{0,\perp}$ are the intensities of the parallel and normal components with respect to the orbit plane. Figure 4 shows that the polarization is a slowly varying function of photon energy. In the range of interest here (10-80 keV) it is almost constant.

If the incident and scattered beams are parallel to the orbit plane of the synchrotron (which was the case in our experiments), it can be shown that the polarization factor in the kinematical approximation (equation (6)) is

$$C_p = \tfrac{1}{2}(1 + \cos^2 2\theta_0 - P \sin^2 2\theta_0) \quad . \tag{10}$$

The polarization factor in the dynamical theory (equation (8)) can be written accordingly. Since P is nearly constant one can regard C_p as a function of angle only. This has been done in Fig. 5. It is seen that the polarization factor causes, as expected, a strong intensity reduction in an angular range around $2\theta_0 = 90°$. Obviously, it would be possible to have the polarization factor almost unity for all scattering angles by using a vertical scattering plane. However, in that arrangement the present liquid-nitrogen-cooled detector would limit the accessible angle range.

For accurate structure determinations the incident spectrum, $i_0(E)$, should be known with a high accuracy. The calculations mentioned above involve a number of assumptions regarding the operation of the synchrotron and it would be useful to have some method to measure $i_0(E)$ experimentally: A direct measurement with the detector situated in the primary beam is impossible because of the very high intensity and strong forward scattering from the slit system. Thus one has to resort to indirect measurements using a sample with known scattering properties. This has been done with a good accuracy (R-factor less than 3 %) for Pre-strahlung from a conventional X-ray tube (Coppens et al. 1965). In a similar way Cardas, Glazer, Howard and Bourdillon (1972) have shown that structure factors can be determined with an R-factor in the order of 1 % using synchrotron radiation. So far, our present

measurements using powdered crystals and single crystals have given larger variations. Further work on this problem is under way.

5. Exposure time

Due to the high intensity of the incident beam, the time exposure can be short. Figure 6 presents a diffraction pattern of silicon obtained in 3 s from a sample volume of about 0.4 mm³. As can be seen from the figure, 13 diffraction peaks can still be distinguished although the statistics are rather poor. Table 1 shows the positions of three selected peaks for different times of exposure. In the 3 s run the strong 220 peak is shifted 0.01 keV as compared with the 300 s run. This is equivalent to 0.1% or 0.002 Å in interplanar spacing. The very weak 731/355 peak is shifted 0.16 keV, equivalent to 0.5% or 0.004 Å. Thus even a 3 s exposure yields quite accurate values for the interplanar spacings.

In order to obtain a "number of merit" for integrated intensity measurements, which would depend on exposure time and not on other factors such as spectral distribution of the incident beam, absorption, etc., we have assumed that the integrated intensities measured for the 300 s run are correct. By fitting all 13 peaks for each run to Gaussians we calculated a reliability factor R defined as

$$R = \sum_H |I_H^{(300)} - I_H^{(t)}| / \sum_H I_H^{(t)} \qquad (11)$$

where $I_H^{(t)}$ denotes the area under the hkl peak after background subtraction, and t is the exposure time. Table 1 shows that the R factor is reasonably small, even for the 3 s exposure, but increases rapidly for 1 s. As mentioned before, the statistics for 1 s could be much better if faster electronics were available. These data demonstrate that even at the present stage of development, the energy-dispersive method combined with synchrotron radiation is at least 100 times faster than the angular scan using monochromatic radiation from a conventional X-ray tube.

6. Large scattering vectors

In a structure determination using X-rays one measures the scattered intensity as a function of the scattering vector, $\bar{Q}$, the modulus of which is given by

$$Q = \frac{4\pi}{\lambda} \sin\theta = \frac{4\pi}{hc} E \sin\theta \,. \qquad (12)$$

It is convenient to note that $4\pi/hc$ equals 1.014 $Å^{-1}$/keV, if E is expressed in keV and Q in $Å^{-1}$.

The measured scattering function, $S(\bar{Q})$, is a Fourier transform of the

pair distribution function, $g(\bar{r})$, where $\bar{r}$ is the position vector. Reversely, $g(\bar{r})$ is a Fourier transform of $S(\bar{Q})$. Therefore the accuracy of the determination of $g(\bar{r})$ much depends on the experimental range of $\bar{Q}$. This is especially important for studies of liquids and amorphous materials. Large Q values can be obtained by increasing the scattering angle or the photon energy. In standard angle-dispersive diffraction the maximum obtainable value is about 15 $Å^{-1}$ (calculated for Mo K_α radiation and back scattering). Figures 7 and 8 show diffraction spectra of an iron powder ($2\theta_0 = 44.4^\circ$) and a silicon single crystal ($2\theta_0 = 53.16^\circ$) obtained in the present work and reaching Q values of 18 $Å^{-1}$ and 32 $Å^{-1}$, respectively.

The maximum Q value is limited by the decreasing intensity of the Bragg reflections. It follows from equations (4), (5) and (7), together with (1) and (2), that the integrated intensity is proportional to $|F_H(Q)|^2 Q^{-2}$ in the kinematical approximation (powdered crystals as well as single crystals) and $|F_H(Q)|Q^{-1}$ in the dynamical theory (perfect crystals). As is well known, the structure factor F is proportional to the atomic scattering factor and the Debye-Waller factor. Both these factors decrease with increasing Q. In addition, the incident intensity decreases with increasing energy (Fig. 3). However, as shown in Figs. 7 and 8, the intensity of the synchrotron radiation is large enough to produce measurable diffraction peaks at larger Q values than those obtained with standard methods.

7. Diffraction by samples at elevated temperatures

This type of study is facilitated by the fixed geometry of the energy-dispersive method: only one inlet and one outlet window are needed in the oven described in section 2. The short exposure time due to the high intensity of the synchrotron radiation enables measurements at slowly rising or falling temperatures, provided that the temperature is recorded at the moments when the X-ray patterns are taken. Thus the demand for temperature stabilization can be relaxed. In view of the good stabilization of our oven, we have not taken advantage of this possibility but raised the temperature stepwise. In each step a diffraction pattern was recorded for 300 s. Figure 9 shows some diffraction spectra where the reversible phase transformation alpha to beta manganese can be followed. The diffraction patterns have been indexed using the Powder Diffraction File. Alpha manganese is cubic, $I\bar{4}3\ m - T_d^3$, with 58 atoms in the unit cell. Beta manganese, stable between 710 °C and 1100 °C, is cubic, $P4_132 - O^7$ or $P4_232 - O^6$, with 20 atoms in the unit cell.

The thermal expansion causes shifts in the position of the diffraction peaks. In the linear approximation it follows from equation (1) that

$$Ed_0\left[1 + \alpha(t-t_0)\right]\sin\theta_0 = \tfrac{1}{2}hc \ , \qquad (13)$$

where α is the linear thermal expansion coefficient, t the temperature, and d_0 the interplanar spacing at temperature t_0. Analysis of the data for alpha manganese in the temperature range 25-690 °C resulted in a mean value of the thermal expansion coefficient, $\bar{\alpha}$ = (33.2±0.9)x10^{-6} K^{-1}. Similarly, $\bar{\alpha}$ = (49±10)x10^{-6} K^{-1} was obtained in the range 730-770 °C (only a few observations). These values are in good agreement with those given in Gmelins Handbuch (1973).

In a similar way the irreversible structural changes accompanying the chemical reaction MnO_2 to Mn_2O_3 around 620 °C were followed.

8. High-pressure diffraction

Also in this case the fixed geometry of the energy-dispersive method is of great value. The high intensity of synchrotron radiation makes it possible to study very small samples within reasonable times. In addition, the use of high-energy photons reduces the absorption in the sample and the high-pressure cell.

The experiments in the present work were performed using a diamond anvil squeezer (Fig. 10) capable of pressures up to 250 kbar. The pressure

gradient in the centre of the cell is reduced by a platinum gasket. The sample diameter is about 0.5 mm. The sample thickness is reduced to 0.1 mm or less by applying the pressure. Thus the amount of material giving rise to the diffraction pattern is very small, of the order of 0.02 mm^3.

Figure 11 shows diffraction patterns of tellurium oxide (TeO_2) before and after the application of a pressure of 80 kbar. In addition to the TeO_2 diffraction lines, one observes Pt diffraction lines from the gasket as well as Te and Pt fluorescence lines. A broadening of the TeO_2 lines is noticed in the high-pressure spectrum. This is due to a tetragonal to orthorhombic phase transformation. A closer inspection (using a more suitable energy calibration of the multichannel analyser) shows, for instance, that the 012 peak splits into two close peaks, namely 012 and 102.

Figure 12 and 13 exemplify other effects that can be observed at high pressures. Figure 12 shows for AgI that the relative intensities of silver and iodine fluorescence change after applying pressure. This is due to pressure diffusion caused by a gradient of chemical activities generated in the pressure gradient of the diamond cell. In Fig. 13 the relative volume changes of FeS, evaluated from lattice constants as a function of pressure, are plotted in order to determine the compressibility H. We obtained

$H = 2.43 \cdot 10^{-6}$ bar^{-1}, which is, however, somewhat higher than the theoretical value of $0.96 \cdot 10^{-6}$ bar^{-1} calculated by Plendl and Gielisse (1969). This may be due to phase transformation and/or pressure diffusion.

9. Time-dependent phenomena

As shown in §5, a useful powder diffraction pattern can be obtained in a few seconds. Therefore slow processes (relaxation times or chemical reaction times of the order of 10 s or longer) accompanied by structural changes can be easily followed. In the case of fast processes (relaxation times of the order of milliseconds and longer) another method must be used. The external field (electrical, magnetic, stress, etc.) must be repetitively pulsed, the X-ray pattern being taken at a certain time, t, after the pulsed field has been applied or removed. By varying t, the structure changes in the course of time can be followed.

If a synchrotron is used as an X-ray source, the fact that X-rays are only produced for a short time in each cycle, as already mentioned in section 2, should be carefully considered. Moreover, both the intensity and the spectral distribution of the emitted X-rays change even in the course of this short period. For these reasons, a storage ring may be a better source though the X-rays emitted are also pulsed. However, the frequency of pulsation is much higher and semiconductor detector systems with their present time resolution are not sensitive to these pulsations and "see" a radiation continuous in time. In order to provide the necessary pulses for measurements of time-dependent phenomena, use should be made of a mechanical chopper or the electronic recording system should be pulsed.

The pulse technique was suggested already in the early sixties in connection with the neutron time-of-flight diffractometry invented at that time (Buras & Leciejewicz, 1964). The realization of this idea was recently reported (Niimura & Muto, 1973, 1975). A similar experiment using synchrotron radiation is now under way*).

10. Conclusions

It has been shown that synchrotron radiation is an ideal X-ray source for energy-dispersive diffractometry. The method is especially suited for fast structure identification and for the study of phase transformations and chemical reactions at high temperatures and/or high pressures. The resolution and maximum count rate are at present limited by the detector system only. Scattering can be observed for larger scattering vectors than in stan-

---

*) In collaboration with Dr. N. Niimura, Tohoku University, Sendai, Japan, at present at the Research Establishment Risø, Roskilde, Denmark.

dard methods. Structural changes can be followed in statu nascendi for time constants of the order of 10 s or more. Faster processes (time constants of the order of ms and larger) can be studied by applying a repetitively pulsed external field synchronized with the X-ray pulses.

Acknowledgements

We would like to express our thanks to DESY, in particular to Prof. G. Weber, Research Director, for the permission to perform the test, to Drs. C. Kunz and E.E. Koch for their daily interest for the work and help, and to Mr. W. Schmidt for technical help. We would like also to thank Prof. A. Lindegaard-Andersen for encouragements and discussions. The substantial technical help of Mr. F. Ferrall is greatly appreciated.

This work would not be possible without the financial support of Danish Natural Sciences Research Council which we gratefully acknowledge.

References

ALSTRUP, O., GERWARD, L., SELSMARK, B., BURAS, B. & STAUN OLSEN, J. (1975). Acta Cryst. A31, 5234.

BORDAS, J., MUNRO, I.H. & GLAZER, A.M. (1976). Nature, 262, 541-545.

BORDAS, J., GLAZER, A.M., HOWARD, C.J. & BOURDILLON, A.J. (1977). Phil. Mag. 35, 311-323.

BURAS, B. & LECIEJEWICZ, J. (1964). Phys. stat. sol. 4, 349-355.

BURAS, B., CHWASZCZEWSKA, J., SZARRAS, S. & SZMID, Z. (1968). Report 894/II/PS, Institute of Nuclear Research, Warsaw.

BURAS, B. & GERWARD, L. (1975). Acta Cryst. A31, 372-374.

BURAS, B., STAUN OLSEN, J., GERWARD, L., SELSMARK, B. & LINDEGAARD-ANDERSEN, A. (1975). Acta Cryst. A31, 327-333.

BURAS, B., STAUN OLSEN, J. & GERWARD, L. (1976). Nucl. Instr. and Meth. 135, 193-195.

COLE, H. (1970). J. Appl. Cryst. 3, 405-406.

GIESSEN, B.C. & GORDON, G.E. (1968). Science, 159, 973-975.

Gmelins Handbuch der unorganischen Chemie, 8. Auflage, System-Nummer 56 (1973), Teil B.

KOCH, E.E. & KUNZ, C. (1974). Synchrotronstrahlung bei DESY, (ein Handbuch für Benutzer).

LAINE, E., LÄHTEENMÄKI, L. & HÄMÄLÄINEN, M. (1974). J. Phys. E: Sci. Instr. 7, 951-954.

NIIMURA, N. & MUTO, M. (1973). J. Phys. Soc. Japan 35 , 628.

NIIMURA, N. & MUTO, M. (1975). Nucl. Instr. and Meth. 126, 87-92.

PLENDL, J.N. & GIELISSE, P.J.M. (1969). Air Force Cambridge Research Laboratories, Hanscom Field, Bedford, Mass. U.S.A. Report AFCRL-69-0426, Paper no. 395.

Figure Captions

Fig. 1. Principle of the energy-dispersive X-ray diffraction method using synchrotron radiation. A-focus point, $2\theta_0$-fixed scattering angle, S_1 and S_2-slits, D-semiconductor detector, and MCA-multichannel pulse-height analyser.

Fig. 2. Resolution in energy-dispersive diffraction spectra. E-photon energy, ΔE-full width at half maximum.

Fig. 3. Calculated spectral distribution of synchrotron radiation. $i_0(E)$-photon flux per unit interval of energy, E_{max} 6.66 GeV-maximum electron energy, j = 7.0 mA-beam current. Slit widths and distance as indicated. The curves show the photon flux (a) in vacuum, (b) after passage through a 0.25 mm thick beryllium foil, (c) after passage through the same beryllium foil and 1 m path in air.

Fig. 4. Calculated polarization, P, of synchrotron radiation as a function of photon energy. E_{max} = 6.66 GeV. Same slit as in Fig. 3.

Fig. 5. Calculated polarization factor in the kinematical approximation as a function of the scattering angle. E_{max} = 6.66 GeV. Same slit

as in Fig. 3. The polarization of the synchrotron radiation has been set to P = 0.88 (Fig. 4).

Fig. 6. Diffraction spectrum of silicon powder. Counting time 3 s. e-escape peak.

Fig. 7. Diffraction spectrum of iron powder.

Fig. 8. Diffraction spectrum of silicon single crystal.

Fig. 9. Diffraction spectra of manganese powder taken at different temperatures. αMn and βMn patterns are indexed for 25° and 770 °C, respectively. The phase transformation can be followed in the spectra for 710°, 720° and 725 °C.

Fig. 10. High-pressure cell with diamond anvil squeezer used in this work.

Fig. 11. Diffraction spectra of TeO_2 powder showing high-pressure phase transformation. (a) Atmospheric pressure. (b) 80 kbar.

Fig. 12. Fluorescence spectra of AgI showing diffusion in pressure gradient. (a) Atmospheric pressure. (b) 50 kbar.

Fig. 13. Compression of FeS.

Table 1. Peak positions and R-factors for silicon powder patterns with various counting time, t.

Silicon powder; Ge detector; Slits: 800 μm/100 μm; distance sample-detector 68 cm.

t / hkℓ	300	100	30	10	3	1	sec
220	11.56	11.56	11.56	11.56	11.57	11.55	keV
511/333	21.26	21.26	21.28	21.27	21.22	21.26	keV
731/355	31.45	31.44	31.46	31.49	31.59	31.29	keV
R	0.0	3.2	6.6	7.0	8.5	26.0	%

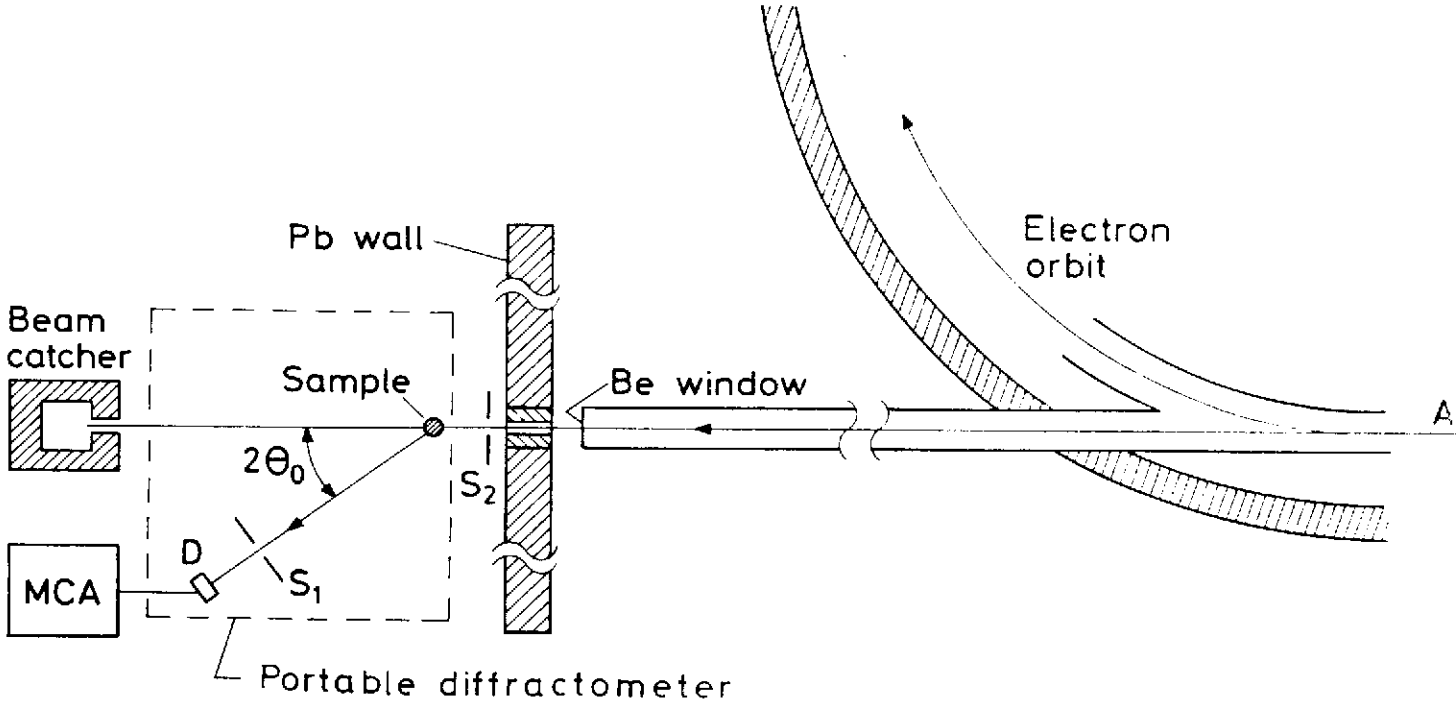
Pb wall
Electron
orbit
Beam
catcher
Sample
Be window
$2\theta_0$
S_2
D
S_1
MCA
Portable diffractometer

Fig. 1.

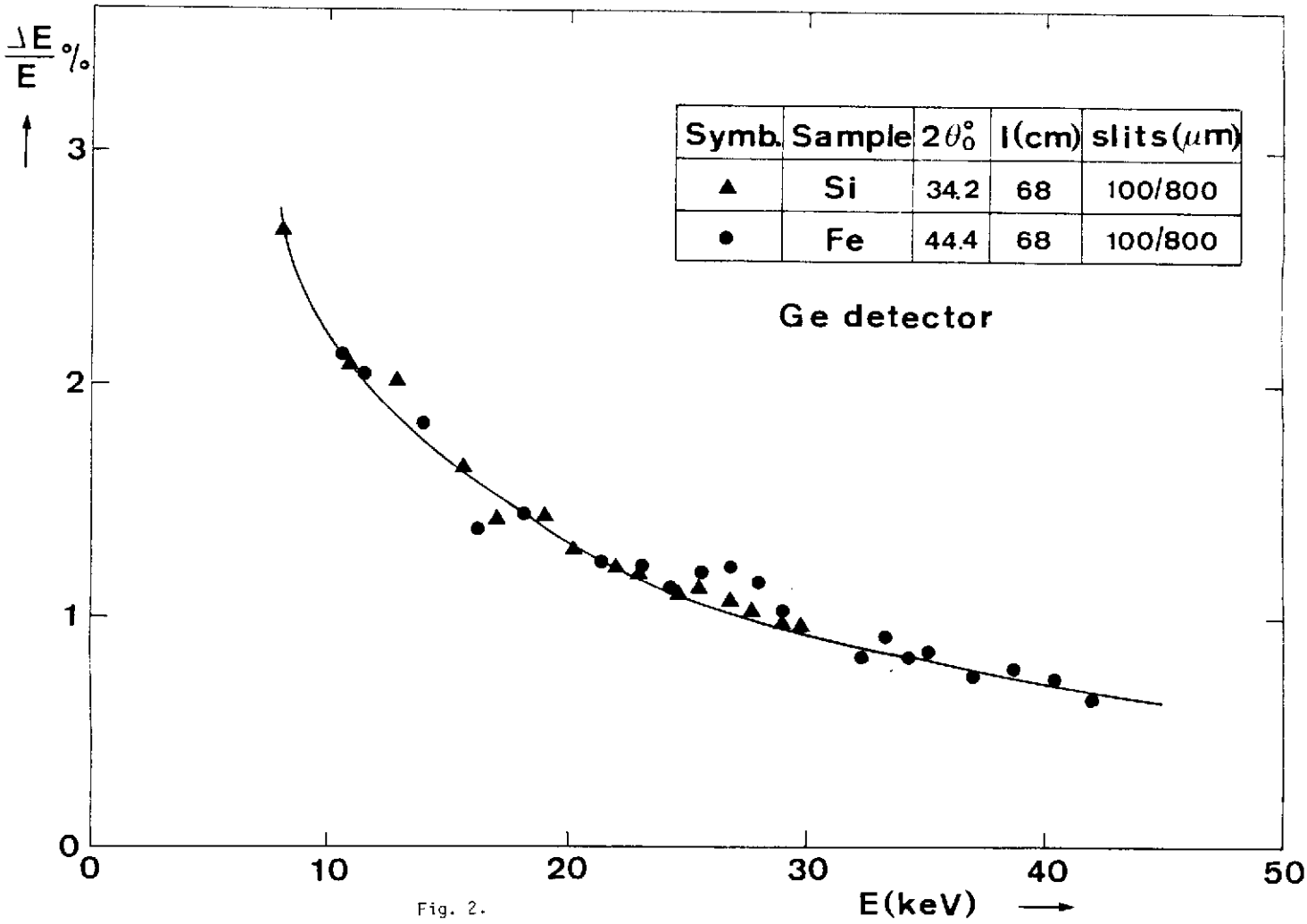
$\frac{\Delta E}{E}$ %
Symb. | Sample | $2\theta_0^\circ$ | l(cm) | slits(μm)
▲ | Si | 34.2 | 68 | 100/800
● | Fe | 44.4 | 68 | 100/800
Ge detector
0
1
2
3
0
10
20
30
40
50
E(keV)

Fig. 2.

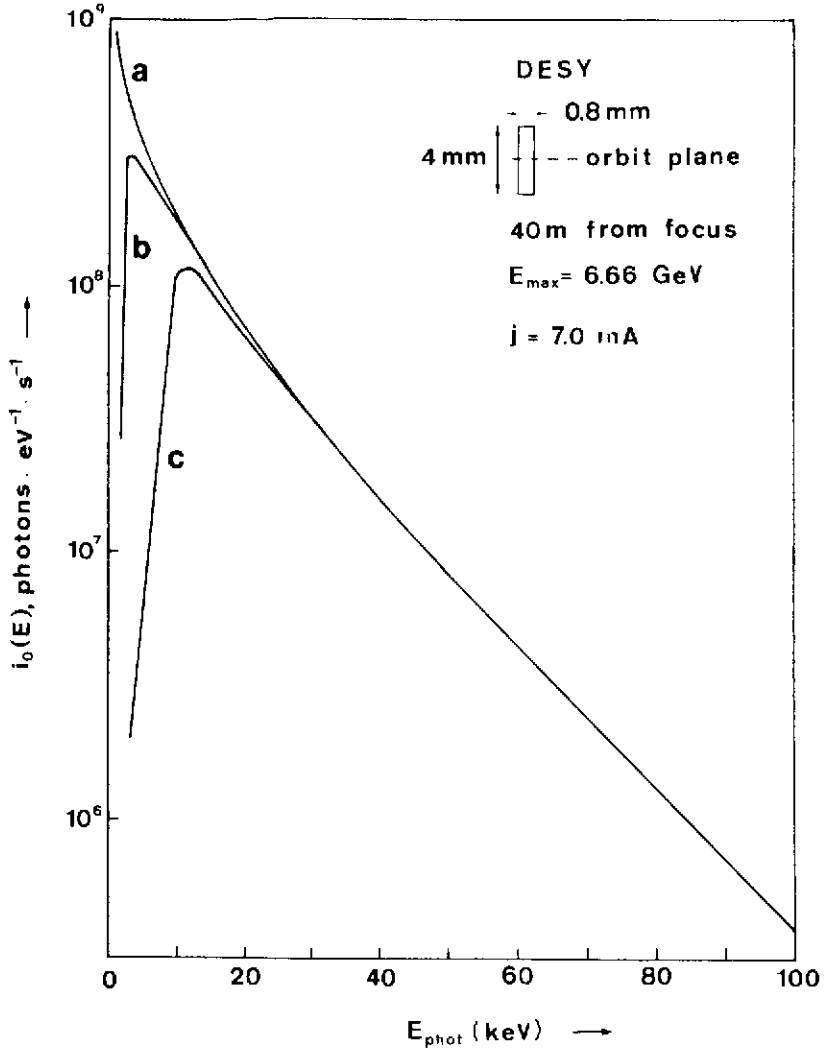
DESY
0.8 mm
4 mm
orbit plane
40 m from focus
E_{max} = 6.66 GeV
j = 7.0 mA
a
b
c
10^9
10^8
10^7
10^6
$i_0(E)$, photons . eV^{-1} . s^{-1} ⟶
0
20
40
60
80
100
E_{phot} (keV) ⟶

Fig. 3.

Fig. 4.

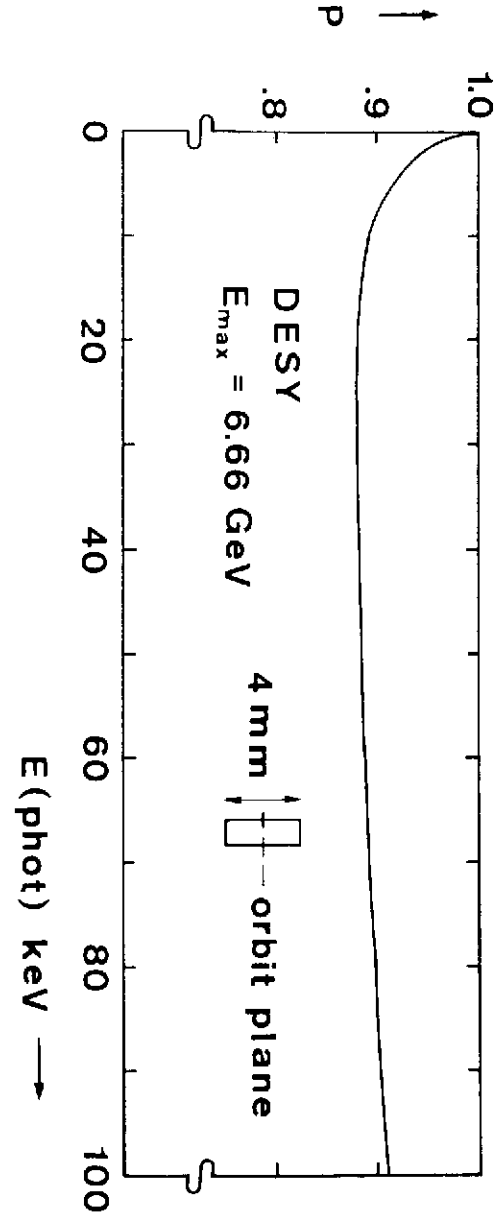
P ⟶
.8
.9
1.0
DESY
E_{max} = 6.66 GeV
4 mm
orbit plane
0
20
40
60
80
100
E (phot) keV ⟶

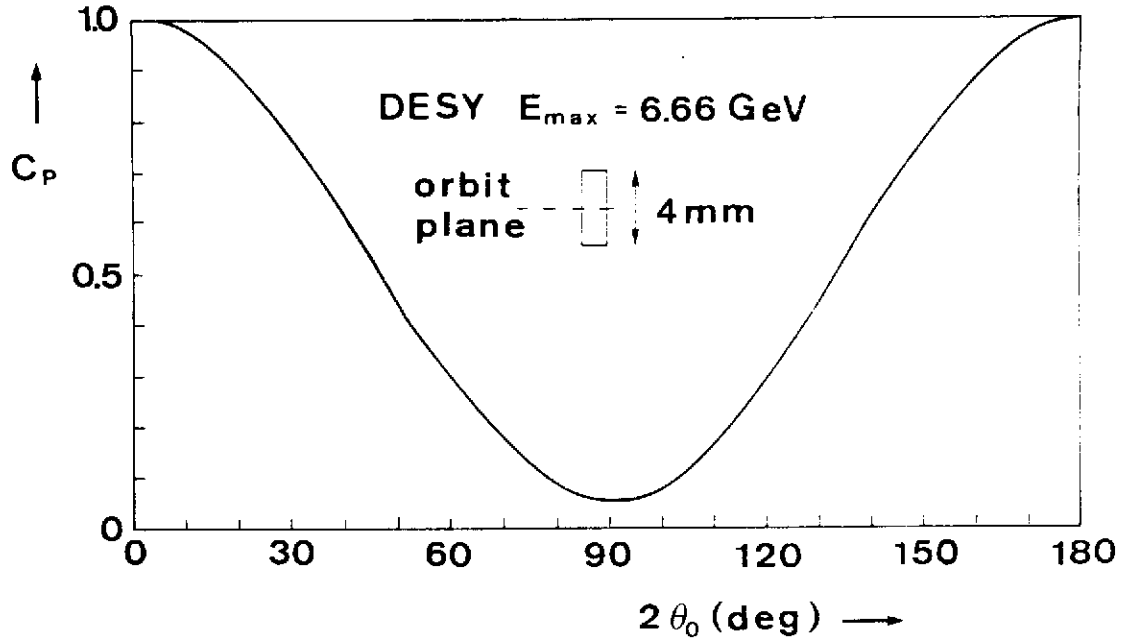
1.0
0.5
0
C_P
DESY E_{max} = 6.66 GeV
orbit plane
4mm
0
30
60
90
120
150
180
$2\theta_0$ (deg) ⟶

Fig. 5.

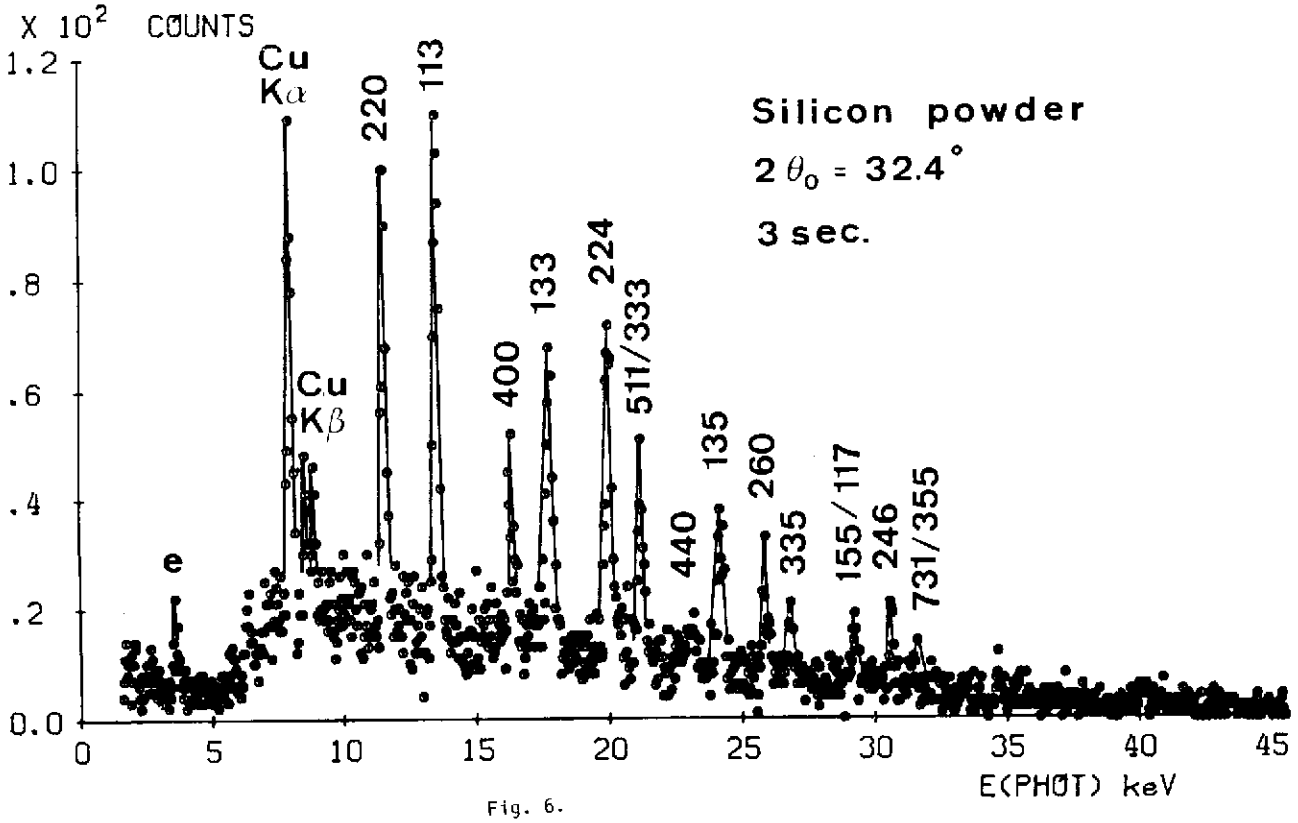
X 10^2 COUNTS
1.2
1.0
.8
.6
.4
.2
0.0
Cu Kα
Cu Kβ
e
220
113
400
133
224
511/333
135
440
260
335
155/117
246
731/355
Silicon powder
$2\theta_0$ = 32.4°
3 sec.
0
5
10
15
20
25
30
35
40
45
E(PHOT) keV

Fig. 6.

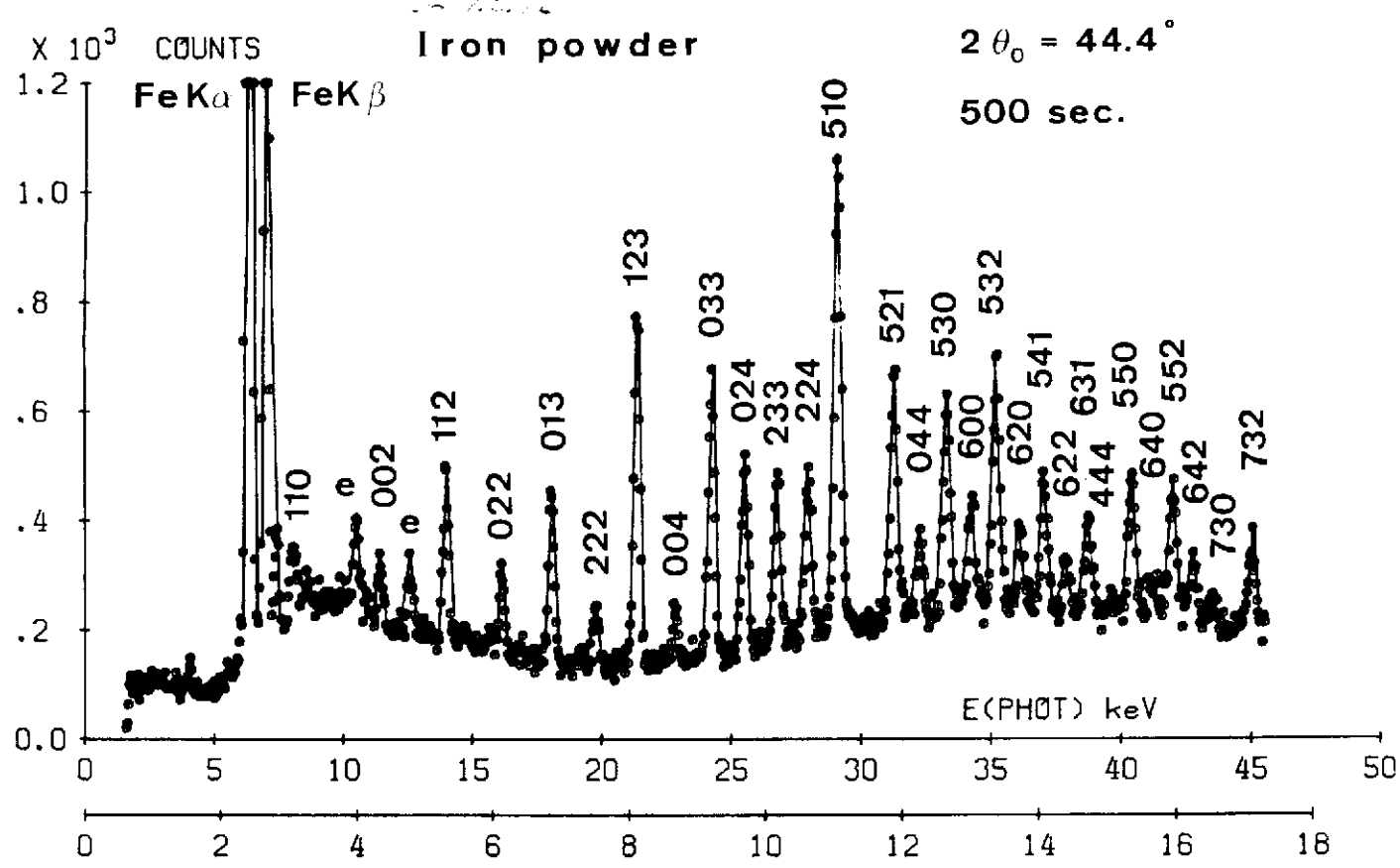

Fig. 7.

$$Q = \frac{4\pi \sin\theta}{\lambda} \quad \text{Å}^{-1}$$

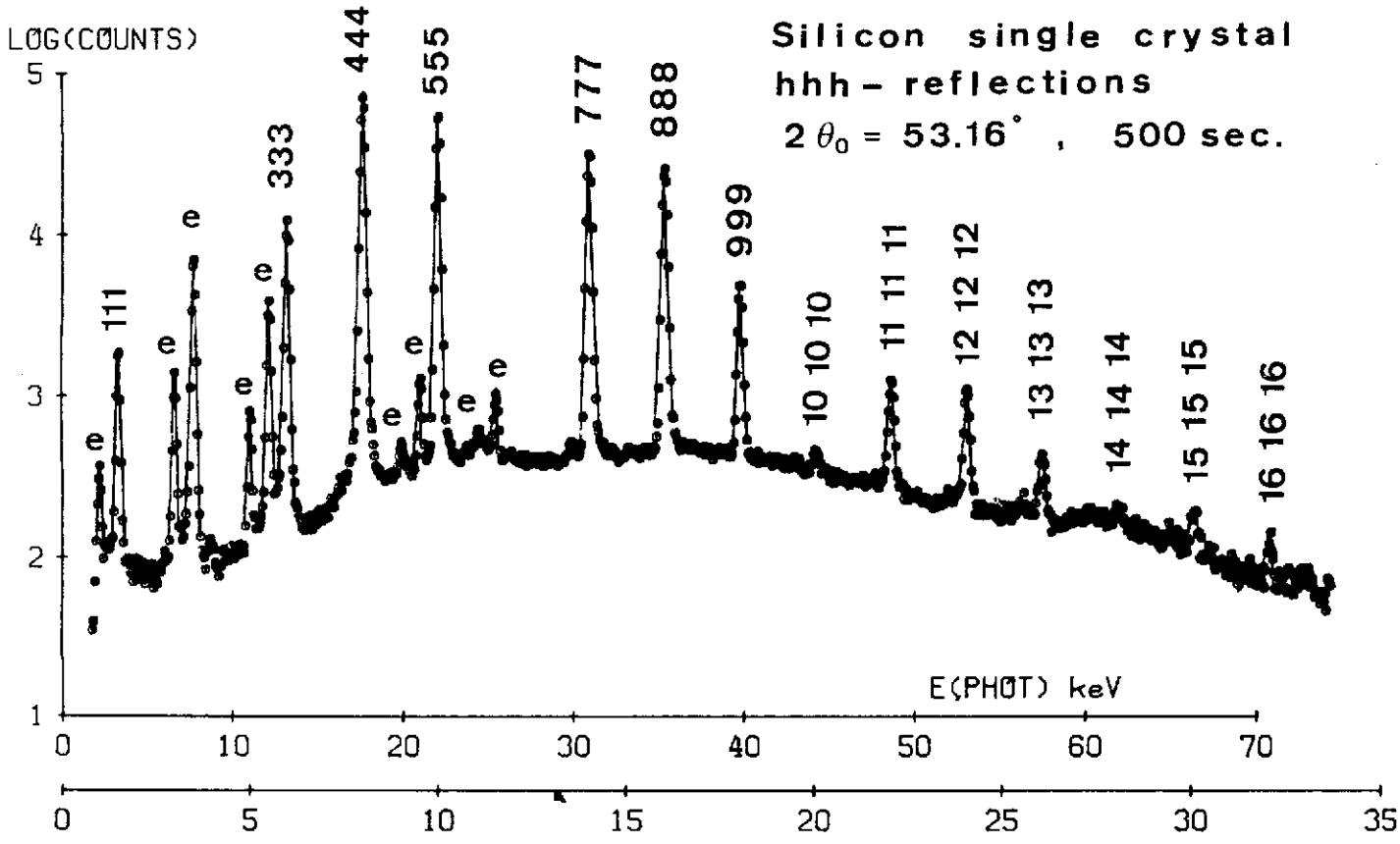

Fig. 8.

$$Q = \frac{4\pi \sin\theta}{\lambda} \quad \text{Å}^{-1}$$

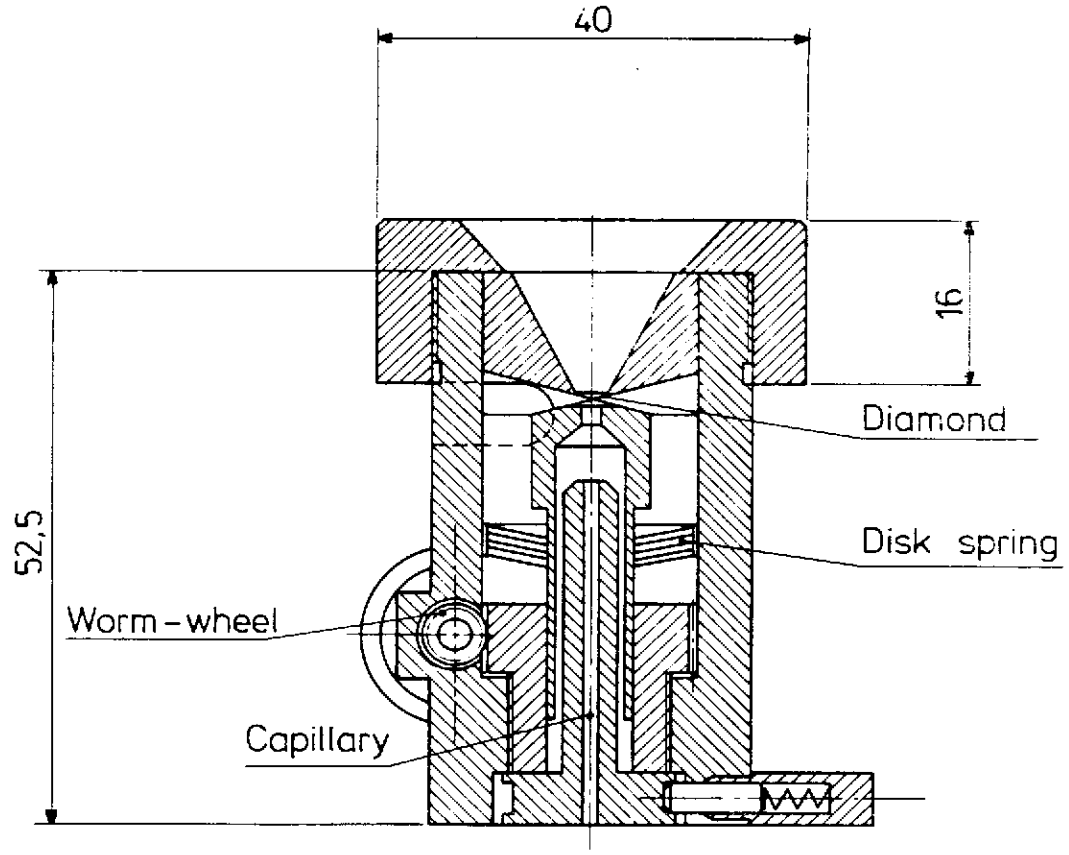
40
16
52,5
Diamond
Disk spring
Worm - wheel
Capillary

Fig. 10

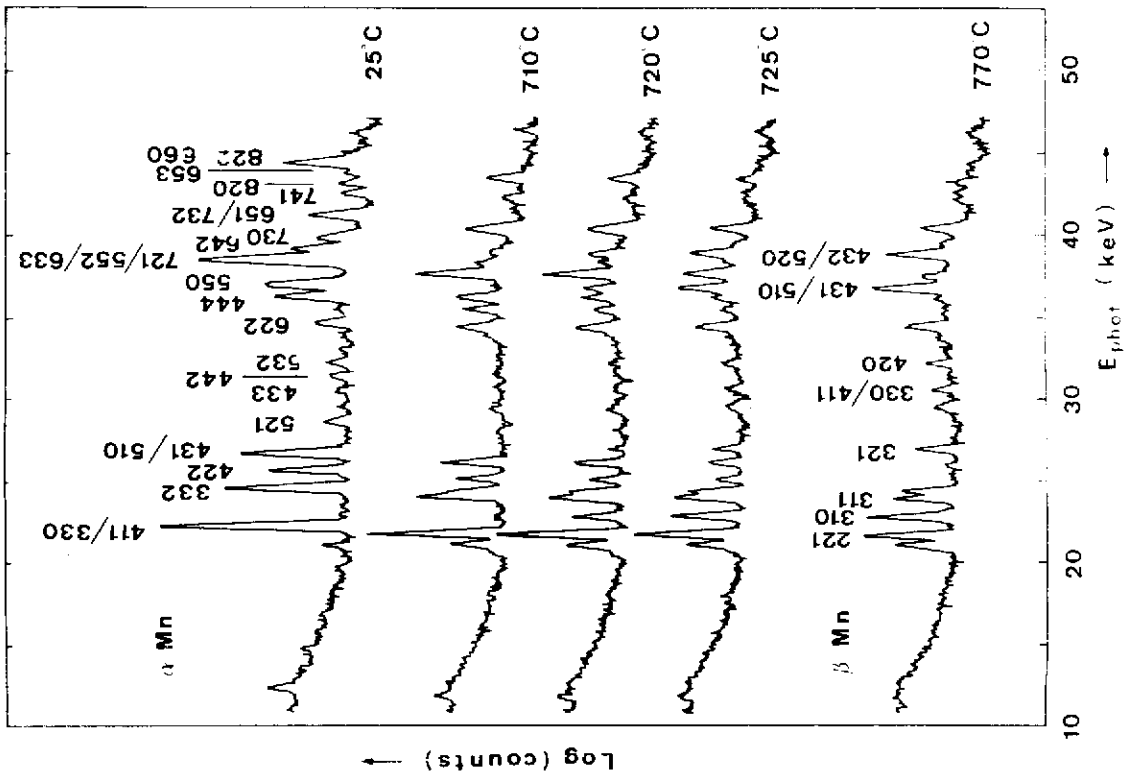
25°C
710°C
720°C
725°C
770°C
α Mn
β Mn
411/330
332
422
431/510
521
433/532
442
622
444
550
730
642
721/552/633
741
820
651/732
822
653
660
221
310
311
321
330/411
420
431/510
432/520
10
20
30
40
50
E_phot (keV) ⟶
⟵ Log (counts)

Fig. 9.

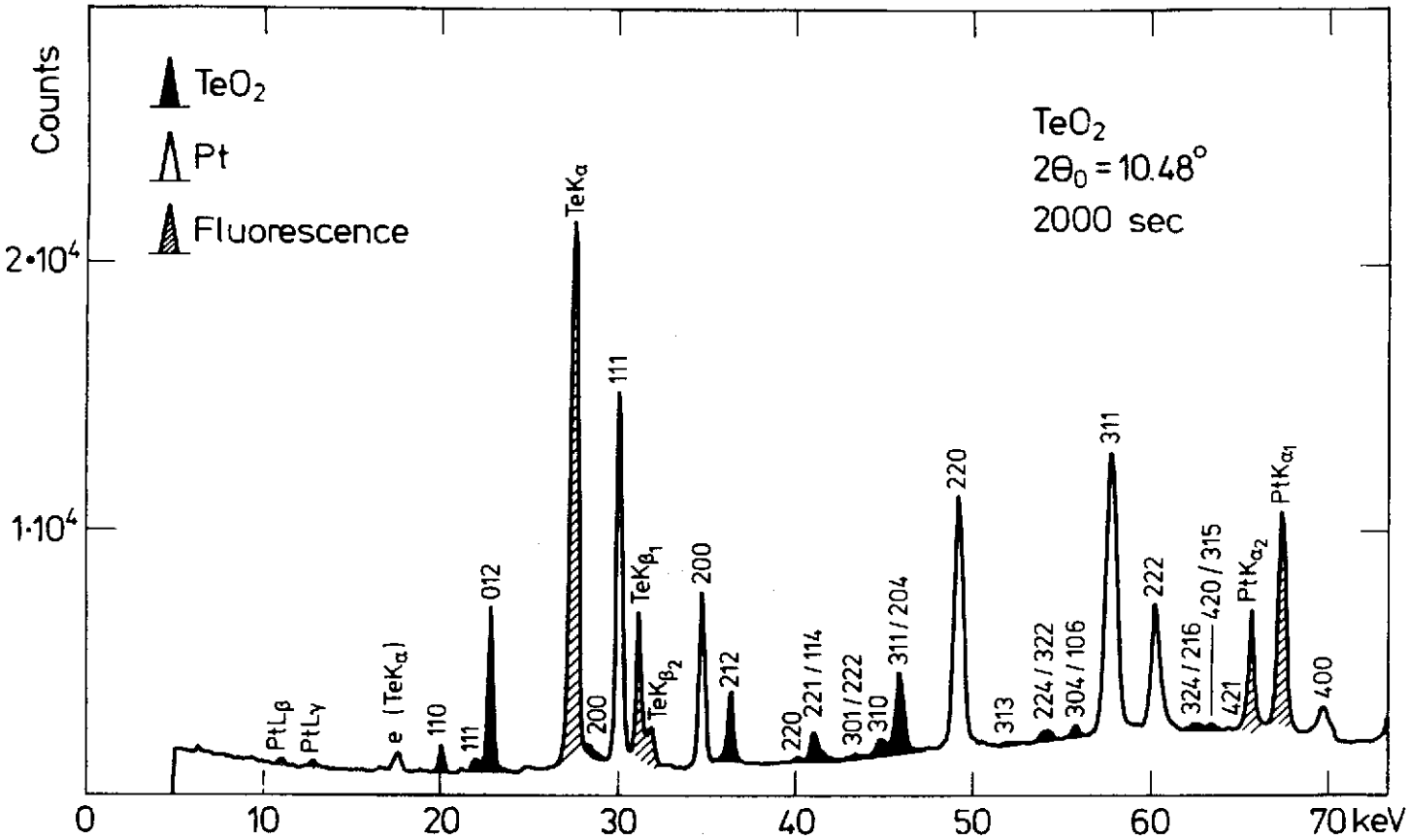

Fig. 11a.

a

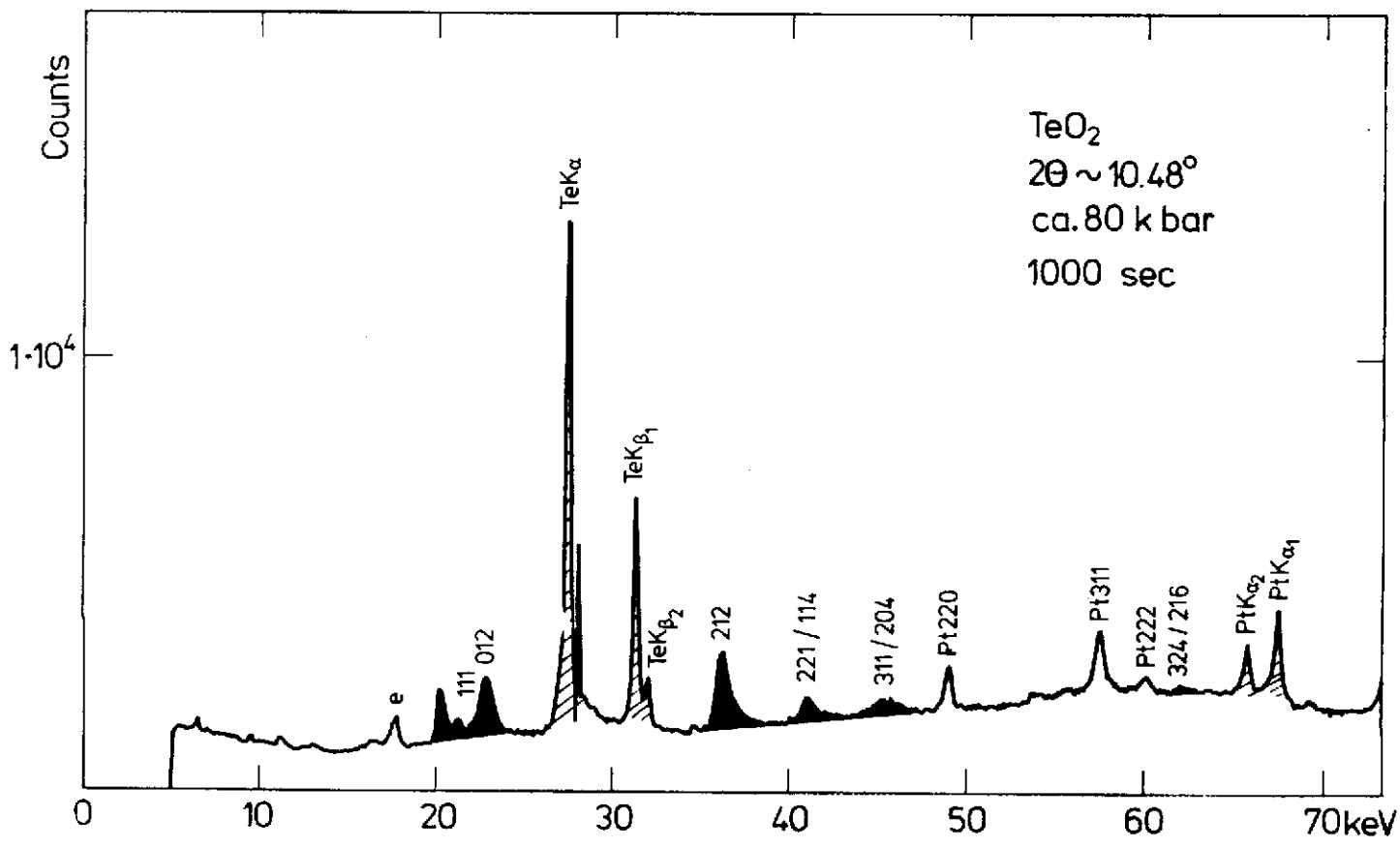

Fig. 11b.

b

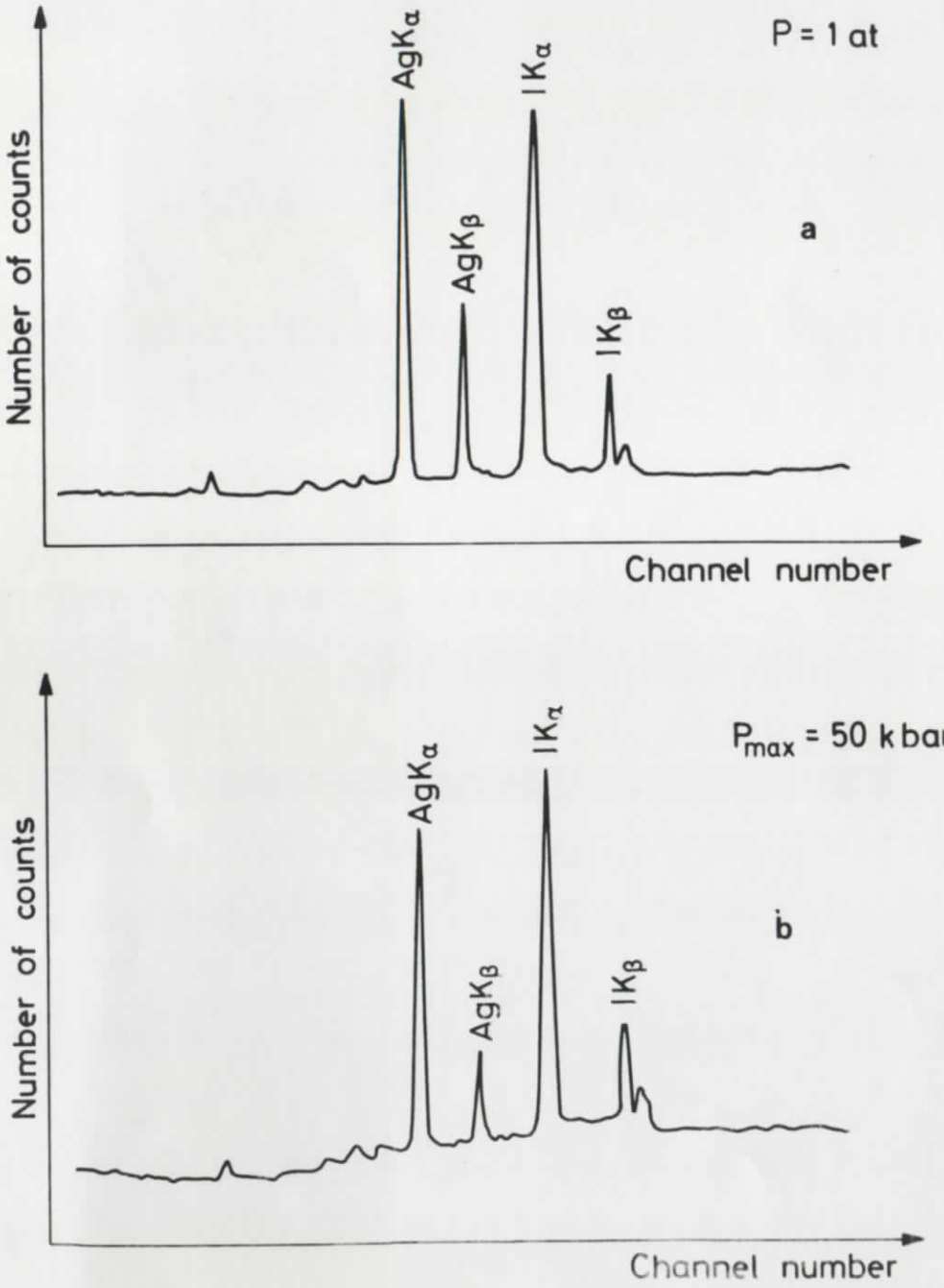

Diffusion in the pressure gradient of a diamond cell
Fluoresence spectrum of AgI

Fig. 12.

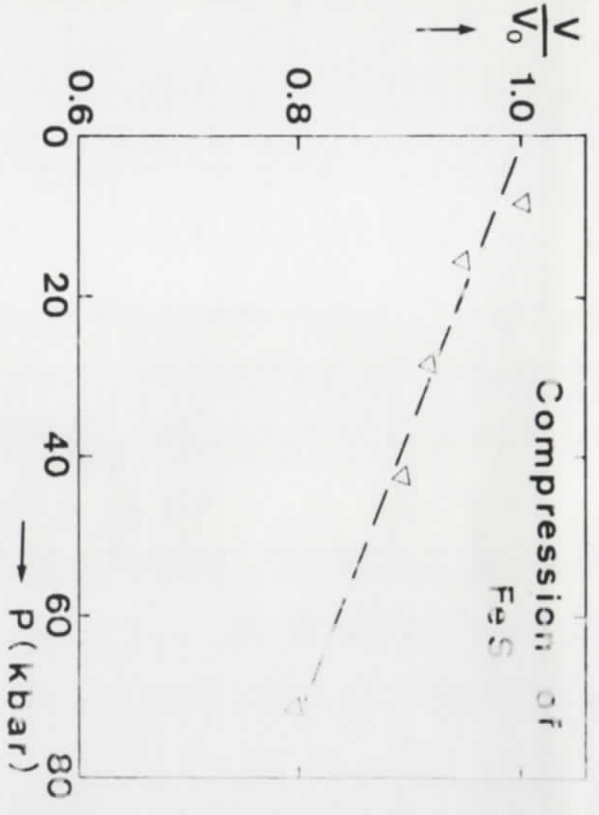

Fig. 13.